Was the extreme Northern Hemisphere greening in 2015 predictable?

A. Bastos, P. Ciais, T. Park, J. Zscheischler, C. Yue, J. Barichivich, R. B. Myneni,
S. Peng, S. Piao & Z. Zhu

Supplementary Methods

Rotated Principal Component Analysis description

The rPCA is a multivariate statistical technique that reduces a given data set *x*, *m*x*n*) into *n* uncorrelated components that explain (in decreasing order) the largest possible fraction of the variance. These components are linear combinations of *x*, obtained by projecting *x* onto each of the eigenvectors of the corresponding covariance matrix. In spatio-temporal fields, each component has a corresponding time-series (PC) and a corresponding spatial field (EOF) of the weighting coefficients (or loadings) (Wallace, 1992).

Usually the goal is to find a $k<<n$ number of components that capture the largest fraction of the total variance in order to study the main variability patterns. It must be noted that the PCA is a purely statistical procedure and therefore the physical meaning the leading modes was initially evaluated.

The long-term NDVI component ($NDVI_{PC1}$) is reconstructed by retaining only the first component of NDVI and projecting it onto the first eigenvector, and $NDVI_{IAV}$ by reconstructing NDVI retaining components 2-16 and projecting them onto the corresponding eigenvectors.

Wallace JM, Smith C, Bretherton CS (1992) Singular value decomposition of wintertime sea surface temperature and 500-mb height anomalies. Journal of climate 5(6):561–576.

Supplementary Figures

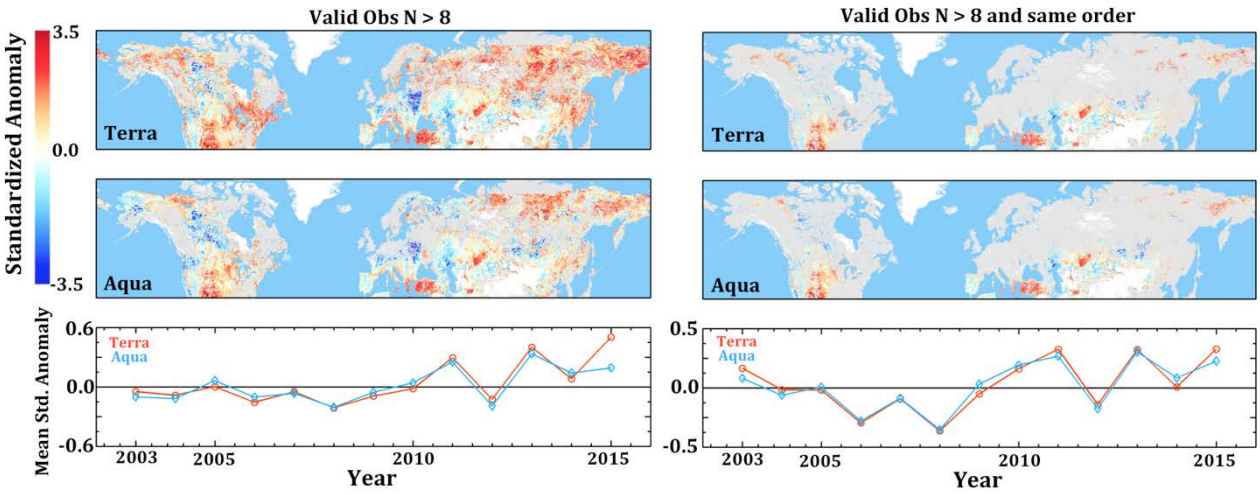

Fig. S1 – Comparison of the 2015 NDVI anomalies during the growing season (Jun-Sep) observed by the MODIS Terra (morning overpass) and Aqua (afternoon overpass) satellites. Since Aqua is only available since 2003, the anomalies are standardized relative to 2003-2014 and we compare only the common period (2003-2015). We limit the analysis to pixels with at least 8 observations over the 13-yr period (left column), and to the ones having valid observations in the same order, guaranteeing that anomalies are directly comparable (right column). Terra provides more valid observations than Aqua over 46.7% of vegetated area. In 2015, Terra presents more valid observations in the mid-latitudes than Aqua (left maps), but the 2015 anomalies for pixels with the same observation number and order largely match (right maps). The lower number of valid observations in Aqua in some regions may be linked to the formation of afternoon summer storms, as the regions with invalid observations largely correspond to high precipitation anomalies shown in Fig. 2. This is reflected in the large difference in NH average NDVI anomaly between the two cases (bottom time-series). However, when comparing the same pixels, NDVI anomalies from Terra and Aqua are consistent.

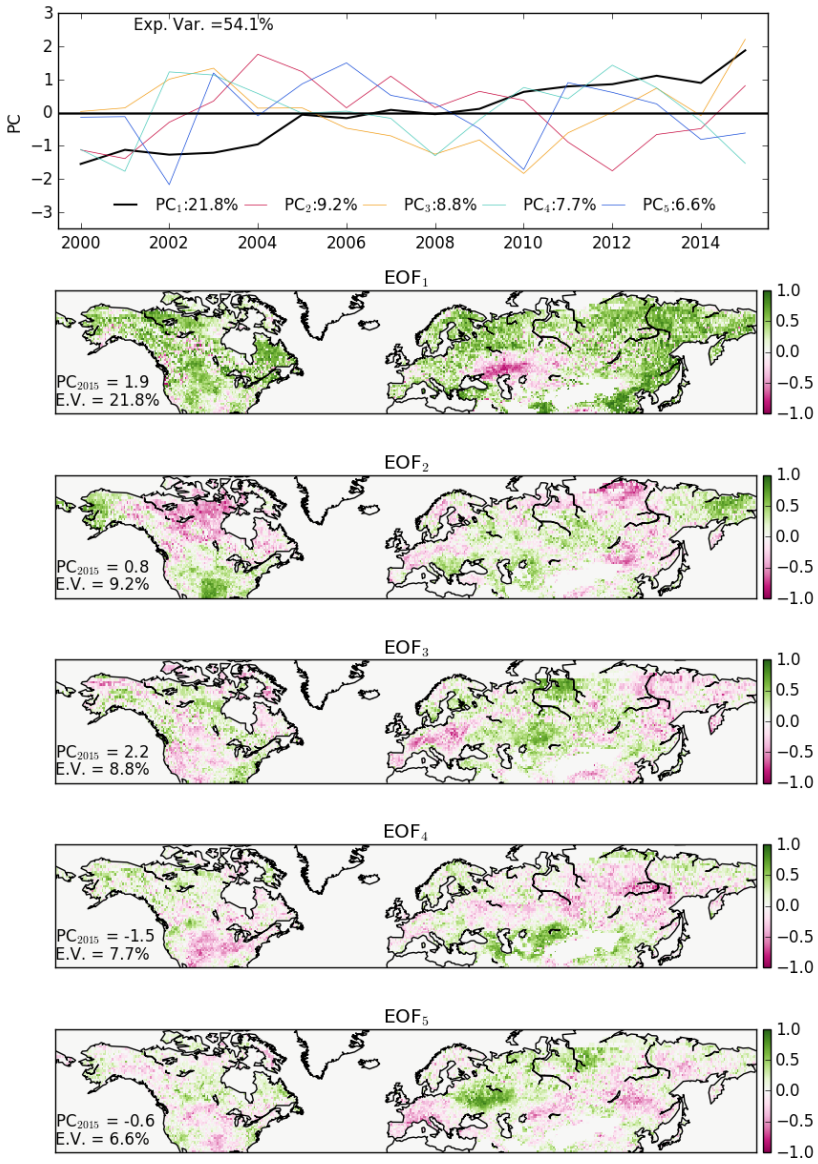

Fig. S2 – Result from the rPCA performed on NDVI, shown for the first five principal components (PC) of Northern Hemispheric NDVI, calculated from PCA of NDVI spatio-temporal fields and corresponding EOFs. The PC score in 2015 and the overall explained variance of the corresponding PC is shown in the lower left of each map. These first five leading modes explain about 54% of NDVI variance.

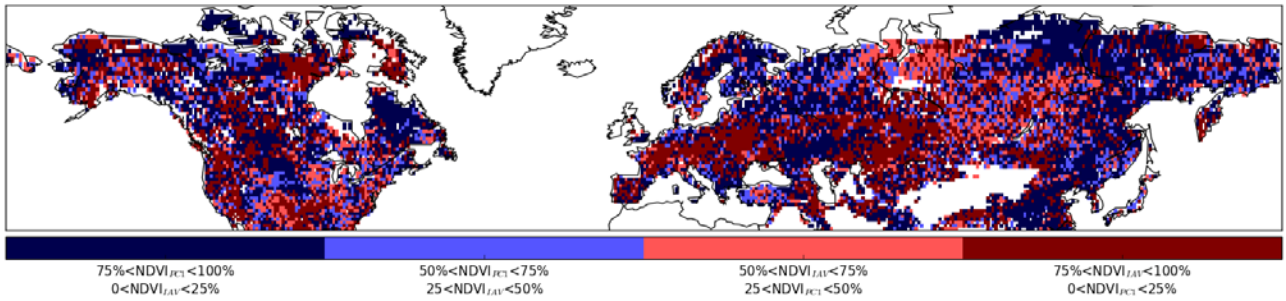

Fig. S3 – Contribution of trend and IAV to the NDVI anomaly observed in 2015. The contribution of trend and IAV is calculated by reconstructing the long-term component ($NDVI_{PC1}$, i.e. trend) and the inter-annual variability component ($NDVI_{IAV}$) for the full period (2000-2015) and calculating the fraction of the anomaly in 2015 that is explained by each component. Blue pixels correspond to regions where the trend explains a larger fraction of NDVI in 2015, while red pixels show regions where IAV explains most of the anomaly in 2015.

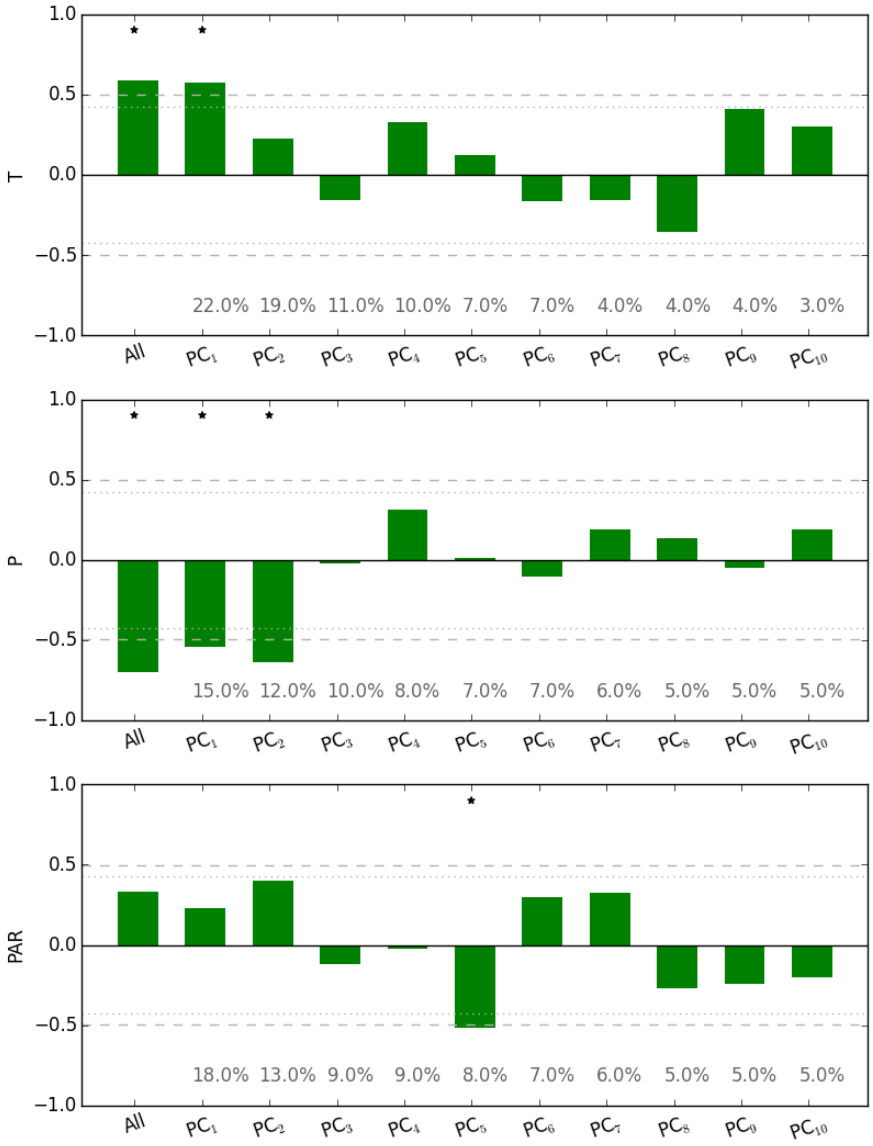

Fig. S4 – Correlation of NH averaged $NDVI_{PC1}$ with hemispheric average temperature (T), precipitation (P) and photosynthetically active radiation (PAR) anomalies during the growing season (JJAS) before PCA decomposition (denoted "All"), and their first ten components calculated from PCA (see also Figure S2 caption). The variables presenting significant correlations were used to select the variables that best explain the variability of $NDVI_{PC1}$.

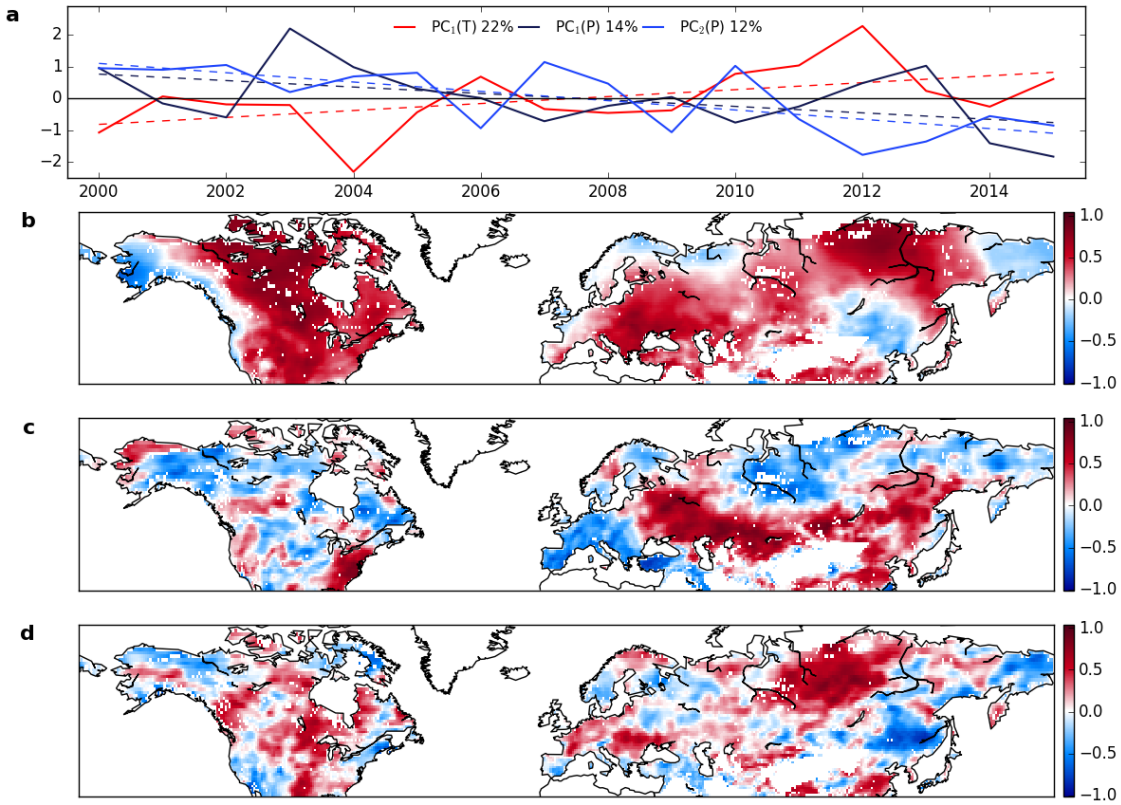

Fig. S5 – Components of climate variables that best explain the variability of $NDVI_{PC1}$. **a)** The time series of $PC_1(T)$, $PC_1(P)$ and $PC_2(P)$ (solid lines) and corresponding linear trend (dashed lines); **b)** $EOF_1(T)$, i.e. spatial distribution of the scores corresponding to $PC_1(T)$; **c)** $EOF_1(P)$, **d)** $EOF_2(P)$. Legend in **a)** indicates the fraction of total variance explained by each component. Positive weights of the EOFs indicate a positive relationship with the corresponding PC and its trend, i.e. warming for $EOF_1(T)$ and drying for $EOF_{1,2}(P)$. The color map is defined so that red matches warming/drying and blue cooling/wetting. $NDVI_{PC1}$ is thus spatially consistent with a generalised warming pattern and with weak Jun-Sep precipitation increase in high latitudes and central Europe and decrease over boreal Eurasia and SE USA, where vegetation growth may be stimulated through enhanced radiation.

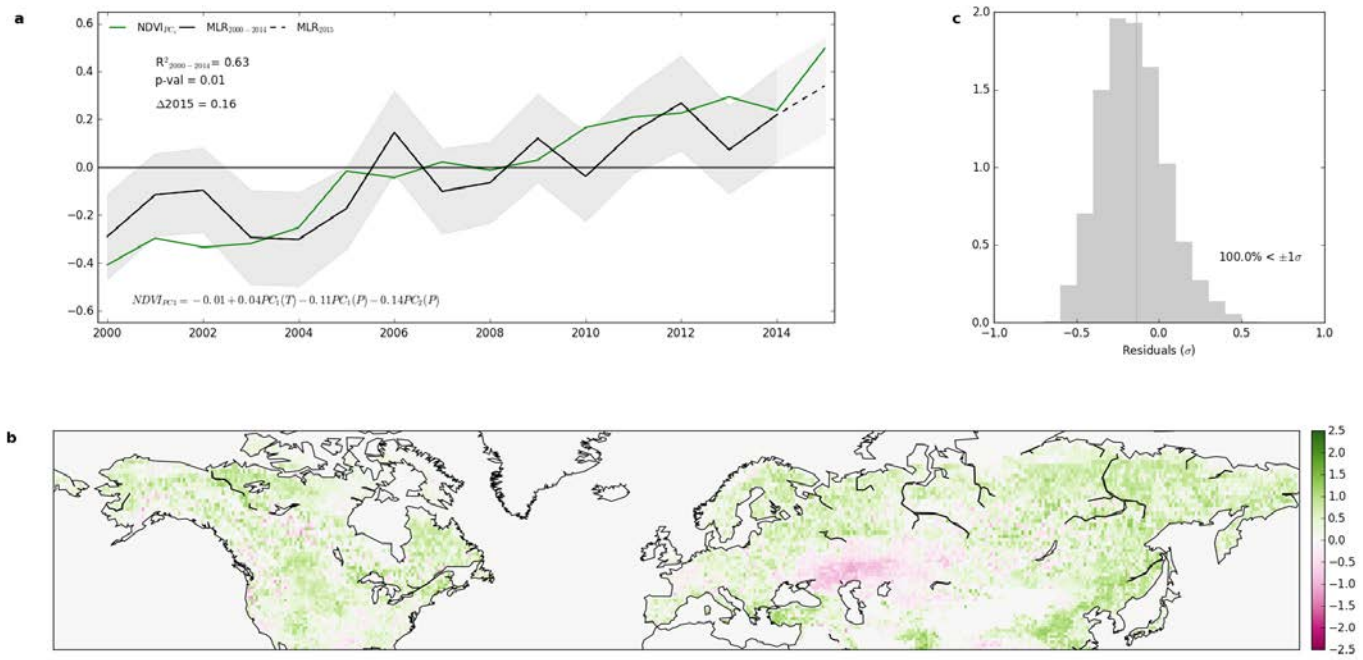

Fig. S6 – Predicting NDVI$_{PC1}$ anomalies in 2015. **a)** NH average NDVI$_{PC1}$ observed (green), corresponding MLR model fit for 2000-2014 (black) and predicted for 2015 (dashed) and 95% confidence interval (grey). The equation of the NH MLR fit, R^2 and *p-value* for the 2000-2014 fit and the deviation between prediction and observation in 2015 are presented in the plot. R^2 adjusted for the number of predictors is 0.53. **b)** pixel-scale predicted NDVI$_{PC1}$ for 2015 and **c)** the corresponding distribution of the residuals.

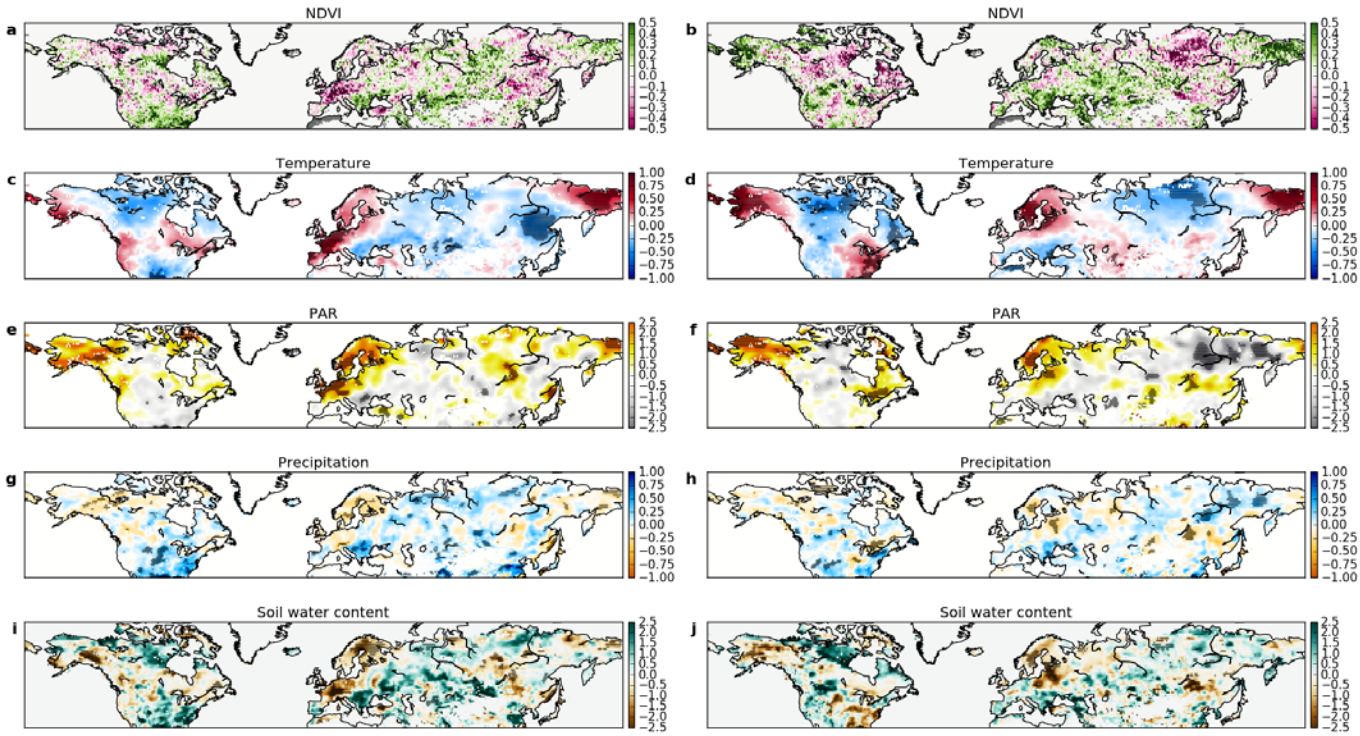

Fig. S7 – Sensitivity of vegetation and climate to PDO and AMO variability between 2000-2014. Coefficients of the regression $NDVI_{IAV} = a\text{PDO} + b\text{AMO}$ calculated over the period 2000-2014 shown in panels **a)** and **b)** respectively. These coefficients are used to predict the spatial distribution of the 2015 anomaly in Fig 3c. Sensitivity of climate variables (JJAS average, detrended) to PDO and AMO, **c)** and **d)** temperature (^{o}C), **e)** and **f)** PAR ($W.m^{-2}$), **g)** and **h)** precipitation ($mm.day^{-1}$) and **i)** and **j)** SWC (%). The areas where significant correlations are found ($p<0.1$) are highlighted by markers. Since AMO was mostly positive during the period 2000-2014, the sensitivity coefficients shown in panels, **b,d,f,h** and **j** relates mostly to high/low positive AMO phases.

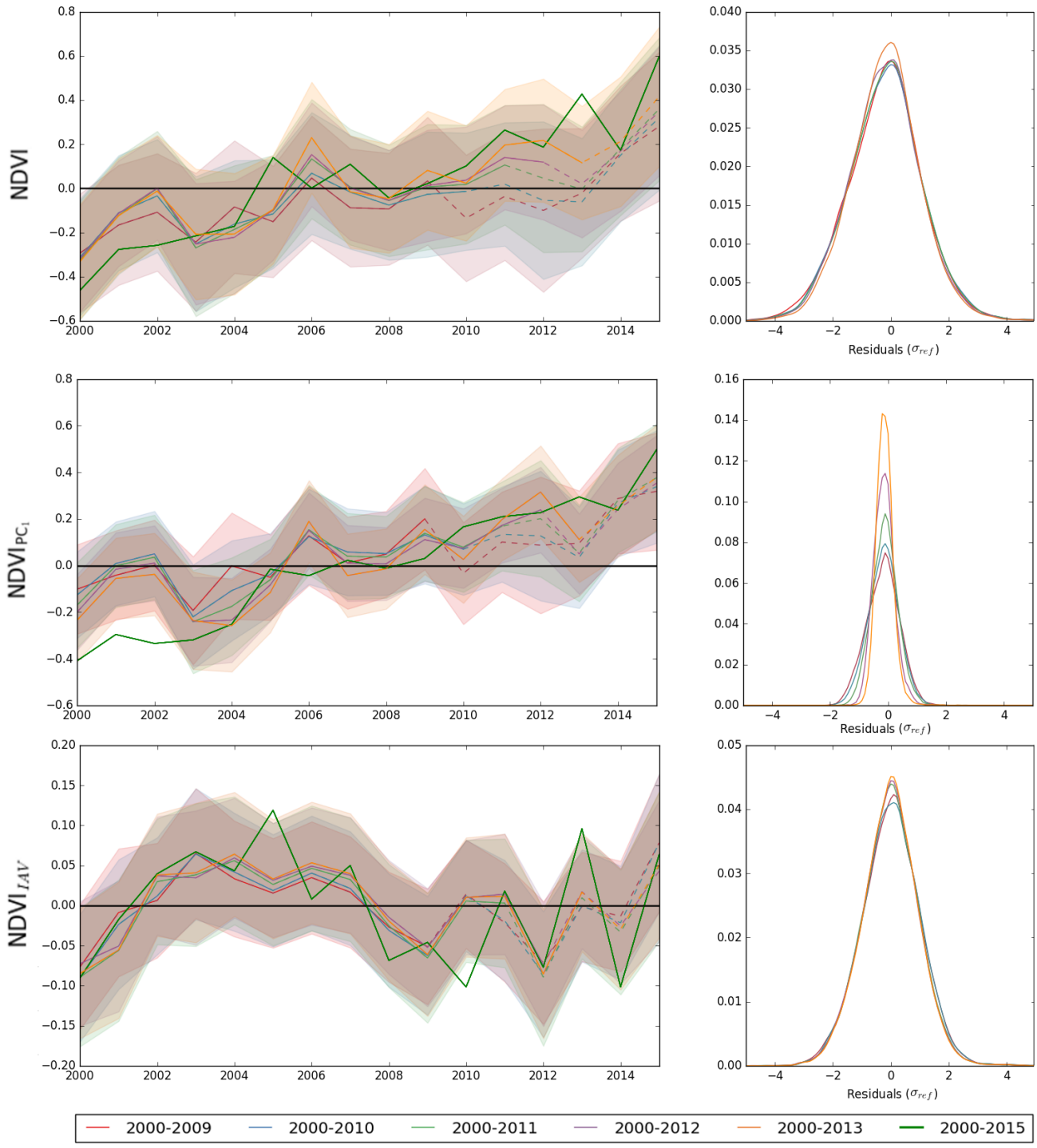

Fig. S8 – Prediction of NDVI using shorter training periods for the full time-series (NH NDVI, top panel), for the long-term trend ($NDVI_{PC1}$, middle panel) and inter-annual variability ($NDVI_{IAV}$, bottom panel). On the top left panel, hemispheric average NDVI anomaly between 2000-2015 (green) and predicted NH NDVI anomaly during 2000-2015 calculated from the two MLR models on $NDVI_{PC1}$ and $NDVI_{IAV}$, shown in the middle and bottom panels respectively. The PCA decomposition of NDVI and climate was performed for variable number of observations n=10, 11, 12, 13, 14 (2000-2009, 2000-2010, 2000-2011, 2000-2012, 2000-2013 respectively) and MLR models using the same predictors (leading modes of T and P for $NDVI_{PC1}$ and PDO and AMO for $NDVI_{IAV}$) were fit. On the right side, the statistical distribution of the model residuals in 2015 is shown for each MLR fit. In general, the MRLMs are able to capture NH NDVI anomalies and variability (within the uncertainty range). As expected, the fit improves with longer training periods, although NDVI in some years can not be captured by the MLRMs (e.g. 2005 and 2013).

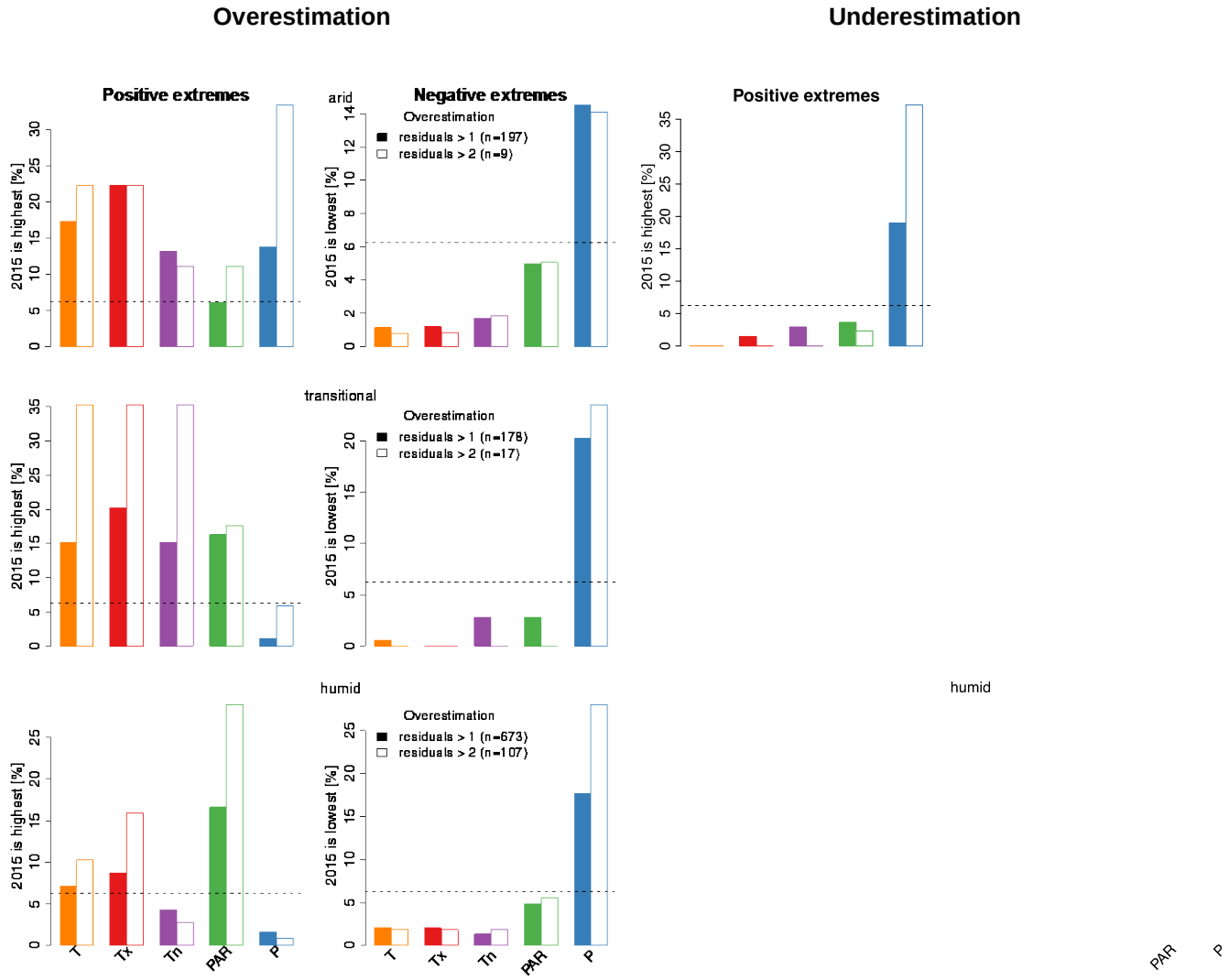

Fig. S9 – Analysis of the climate extreme occurrence in pixels with very high residuals (shown in Fig. 4b, to be compared with Fig. 4c). For residuals exceeding 1σ (filled bars) and 2σ (open bars), we compute the percentage of pixels where climate variables (T, minimum temperature (Tn), maximum temperature (Tx), PAR, P) in 2015 are highest (i.e., positive extremes) and lowest (i.e., negative extremes). If 2015 is to be the most extreme for a given climate variable, the expected fraction of pixels would be 6.25% if there was no association between NDVI and that climate variable (denoted by the dashed horizontal line). Arid, transitional and humid areas (as defined in Greve et al. (2014) and shown in Figure 4c) are analyzed separately in the top, middle and bottom panels respectively.

Supplementary Table 1

Correlation between the different components of Northern Hemispheric NDVI and the leading atmospheric circulation patterns of the NH (NAO, EA) and the three main coupled atmosphere-ocean coupled variability modes that influence global climate (ENSO using the MEI index, PDO, AMO) during DJF and JJAS. The bold values and the asterisks indicate the significance of correlations ($p<0.1$ and $p<0.05$, respectively). NDVIIAV is significantly correlated with climate variability modes, especially in winter. The first component of NDVI, does not correlate with any climate variability pattern, as it is linked to the long-term trend. On the contrary, the first four components linked with IAV (PC2-5) present significant correlations with at least one index.

DJF	**NAO**	**EA**	**MEI**	**PDO**	**AMO**
$NDVI_{IAV}$	0.06	0.03	0.38	**0.48**	**0.57***
PC1	0.07	0.00	0.08	0.11	0.00
PC2	-0.13	-0.03	**0.58**	**0.48**	**0.54***
PC3	**0.53***	0.03	0.22	**0.52***	-0.04
PC4	-0.37	-0.10	0.30	-0.11	0.42
PC5	0.16	**-0.49**	-0.20	0.03	0.10
JJAS	**NAO**	**EA**	**MEI**	**PDO**	**AMO**
$NDVI_{IAV}$	0.35	0.04	0.14	**0.45**	-0.09
PC1	-0.18	0.06	0.23	0.06	0.21
PC2	0.15	-0.25	0.11	**0.64***	0.12
PC3	0.02	0.34	**0.61**	**0.59***	-0.26
PC4	**0.43**	**-0.51***	-0.20	-0.12	0.29
PC5	0.25	0.20	-0.08	-0.12	0.30